Progress In Electromagnetics Research, PIER 74, 291–307, 2007

RECONSTRUCTION OF 2D PEC TARGETS USING LIMITED SCATTERED INFORMATION

J. Wu and T. J. Cui

Institute of Target Characteristics and Identification
State Key Laboratory of Millimeter Waves
Department of Radio Engineering, Southeast University
Nanjing, 210096, P. R. China

Abstract—An efficient method is proposed in this paper to reconstruct the shape of a two-dimensional perfectly electrically conducting (PEC) target using limited scattered information. Based on the physical optics approximation, a Fourier transform relation has been obtained between the PEC target and the scattered fields. In theory, all scattered-field data are required for the reconstruction in the whole angle range (from 0 to 2π) and in the whole frequency range (from 0 to ∞). However, such data are impossible in practical applications. In this paper, we have discussed the influence of limited frequencies and limited incident angles on the imaging, where a Pade interpolation technique has been developed to obtain the scattered information in the whole angle range from limited-angle information. In order to overcome the ill-posed problem in the interpolation, the Tikhonov regularization has been used. Reconstruction examples are given to validate the efficiency of the proposed approach.

1. INTRODUCTION

The electromagnetic scattered information of a perfectly electrically conducting (PEC) target has been popularly used in the modern radar system. Among all kinds of target detecting theories, the target imaging has received increasing interest because it can provide more particular details in the shape and location of the target than others. The theory of inverse scattering for PEC targets has been well studied since 1965 using the physical optics (PO) approximation [1–16]. The most significant contribution to the inverse-scattering theory was established by Bojarski in 1982 [4], where he developed a Fourier transform relationship between the PEC target and the scattered

field. However, such a theory is difficult to be realized in practical applications because all scattered-field information in the whole angle range (from 0 to 2π) and in the whole frequency range (from 0 to ∞) have to be known, which is hard to to be satisfied in practice.

In this work, we mainly discuss the two-dimensional (2D) imaging for PEC targets using limited scattered information. In Section 2, a brief introduction to the inverse scattering theory is given based on the PO approximation, where a Fourier transform relation has been obtained between the PEC target and the scattered fields. In Section 3, the influence of limited frequencies to the imaging is first investigated. Then a Pade extrapolation is proposed to approximate the scattered information in the whole directions around the target using limited measurement data, which can be conveniently achieved in practical applications. In order to overcome the ill-posed problem in the interpolation, the Tikhonov regularization has been used. Finally, reconstruction examples are given to validate the proposed approach in Section 4, followed by the conclusion remarks in Section 5.

2. INVERSE SCATTERING THEORY BASED ON THE PO APPROXIMATION

Consider a 2D PEC target, a PEC cylinder, as shown in Figure 1. When an electromagnetic plane wave is incident upon the target, where the incident magnetic field is parallel to the cylindrical axis, there are electric currents induced on the target. If the electrical size of the object is much larger than the wavelength, we can use the PO

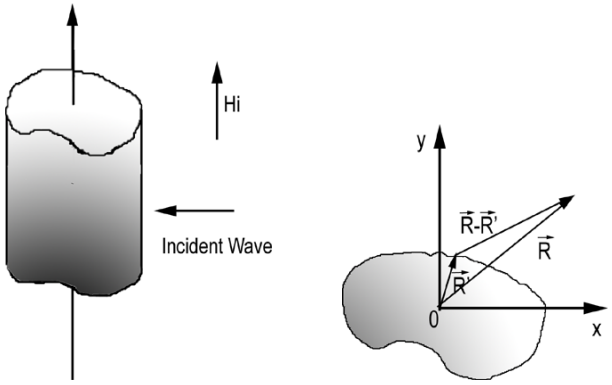

(a) (b)

Figure 1. The scattering model of a PEC cylinder. (a) The overview. (b) The cross section.

approximation to estimate the electric current as

$$\vec{J} = \hat{n} \times \vec{H} = \begin{cases} 2\hat{n} \times \vec{H}_i & \vec{k} \cdot \hat{n} < 0 \\ 0 & \vec{k} \cdot \hat{n} > 0, \end{cases} \quad (1)$$

where $\vec{k}$ is the wavenumber vector, and $\hat{n}$ is the unit normal vector of the PEC target. As shown in Figure 1(a), the incident magnetic field is written as

$$\vec{H}_i = \hat{z} H_0 e^{j\vec{k}\cdot\vec{R}}.$$

Then the scattered magnetic field can be obtained using the far-field approximation

$$\vec{H}_s(\vec{k}_i, \vec{k}_s, \vec{R}) = \frac{1}{2} \int_{\vec{k}_i \cdot \hat{n} < 0} H_0^{(1)}(k_s \left| \vec{R} - \vec{R}' \right|) \vec{H}_i(\vec{R}')(\vec{k}_s \cdot \hat{n}) dl' \quad (2)$$

As shown in Figure 1(b), when the receiving antenna is far from the PEC object, the large-argument approximation of the Hankel function can be used, which yields the scattering field as

$$\vec{H}_s(\vec{k}_i, \vec{k}_s, \vec{R}) = \hat{z} H_0 \frac{\sqrt{i}}{\sqrt{2\pi k_s R}} \int_{\vec{k}_i \cdot \hat{n} < 0} e^{ik_s R} e^{-i(\vec{k}_s - \vec{k}_i)\cdot\vec{R}'} \vec{k}_s \cdot \hat{n} dl'. \quad (3)$$

Now we define a normalized scattered magnetic field as

$$\rho(\vec{k}_i, \vec{k}_s) = \frac{H_s(\vec{k}_i, \vec{k}_s) e^{-ik_s R} \sqrt{k_s}}{\sqrt{i}}.$$

In a mono-static radar system, we have $\vec{k}_s = -\vec{k}_i \equiv \vec{k}$. Considering two opposite incident directions, Eq.(3) can be rewritten as

$$\rho(\vec{k}) - \rho^*(-\vec{k}) = H_0 \frac{1}{\sqrt{2\pi R}} \oint_l e^{-i2\vec{k}\cdot\vec{R}'} \vec{k} \cdot \hat{n} dl'. \quad (4)$$

Applying the Gaussian divergence theorem, Eq. (4) can be reduced to

$$\begin{aligned} \rho(\vec{k}) - \rho^*(-\vec{k}) &= H_0 \frac{1}{\sqrt{2\pi R}} \int_S \nabla \cdot (e^{-i2\vec{k}\cdot\vec{R}'} \vec{k}) ds' \\ &= H_0 \frac{-i2k^2}{\sqrt{2\pi R}} \int_S e^{-i2\vec{k}\cdot\vec{R}'} ds', \end{aligned} \quad (5)$$

where S is the cross section of the cylindrical target. We define a characteristic function of the scatterer as

$$\gamma(\vec{R}) = \begin{cases} 1, & \vec{R} \in S \\ 0, & \vec{R} \notin S, \end{cases} \quad (6)$$

then Eq. (5) can be rewritten in the following form

$$\rho(\vec{k}) - \rho^*(-\vec{k}) = H_0 \frac{-i2k^2}{\sqrt{2\pi R}} \int_{\infty} \gamma(\vec{R}') e^{-i2\vec{k}\cdot\vec{R}'} ds'. \tag{7}$$

Clearly, Eq. (7) describes a Fourier relation. In other words, the characteristic function of the PEC target, $\gamma(\vec{R})$, is the inverse Fourier transform of the following re-normalized scattered field

$$S(\vec{k}) = \frac{\rho\left(\frac{\vec{k}}{2}\right) - \rho * \left(-\frac{\vec{k}}{2}\right)}{k^2 H_0} \times 2\sqrt{2\pi R}.$$

3. RADAR IMAGING USING LIMITED SCATTERED INFORMATION

If we want to perform the inverse Fourier transform shown in Eq. (7), we should know the scattered field information in the whole $\vec{k}$ space. Suppose that the $\vec{k}$ vector is written as $ke^{i\phi}$, where k corresponds to the frequency of incident wave, and ϕ corresponds to the incident angle. Then all frequencies from 0 to ∞, and all incident angles from 0 to 360° should be used. In practical applications, however, we can only obtain limited scattered information, in which $\vec{k}$ is limited in a certain frequency bandwidth, as shown in Figure 2(a), and also we cannot place radars to surround the object. In actual cases, the radars can be only placed in some particular directions, as shown in the black areas in Figure 2(b).

Now we discuss the influence of limited bandwidth as shown in Figure 2(a). Let the scattered data be 0 when $\vec{k}$ is not in the black region ($a \leq |k| \leq b$) shown in Figure 2(a) when we perform the inverse Fourier transform. Then we define the characteristic function computed using such limited bandwidth as $\gamma'(\vec{R})$. Apparently, the relation between $\gamma'(\vec{R})$ and the real characteristic function $\gamma(\vec{R})$ is simply written as

$$\gamma'(\vec{R}) = w(\vec{R}) * \gamma(\vec{R}),$$

in which $w(\vec{R})$ is the inverse Fourier transform of the following function

$$W(\vec{k}) = \begin{cases} 1, & a \leq |k| \leq b \\ 0, & \text{eleswhere.} \end{cases}$$

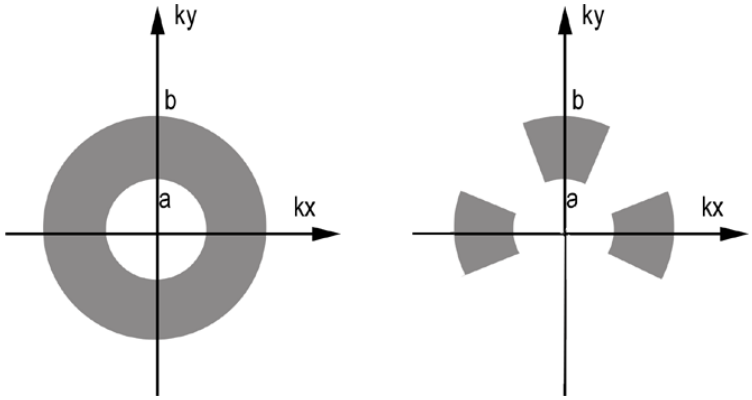

(a) (b)

Figure 2. The scattered field information. (a) Limited frequency bandwidth. (b) Limited frequency bandwidth and limited incident directions.

Clearly, $w(\vec{R})$ has an analytical solution:

$$w(\vec{R}) = \frac{1}{2\pi R}[bJ_1(bR) - aJ_1(aR)].$$

A typical distribution of $w(\vec{R})$ when $a = 0$ and $1/b \ll L$ is shown in Figure 3(a), where L is the object dimension. From this figure, it is easy to see that $w(\vec{R})$ will be a good approximation to the delta function, and furthermore $\gamma'(\vec{R}) \approx \gamma(\vec{R})$ [1]. When $a \neq 0$, for example $b/a = 2.0$, the distribution of $w(\vec{R})$ is shown in Figure 3(b). Obviously, the first sidelobe of $w(\vec{R})$ will affect the object function in performing the convolution. As a result, the outline of the object will have a little defect.

Next, we consider the limitation of the incident directions as shown in Figure 2(b). Suppose that the $\vec{k}$ vector is written as $ke^{i\phi}$, where k corresponds to the incident wave frequency, and ϕ corresponds to the incident angle. As a consequence, the scattered field $H_s(\vec{k})$ is a function of ϕ when k is fixed, which is symbolled as $f(\phi)$. In the practical case, we can only place the radars in some certain directions, as shown in Figure 2(b). In other words, only the scattered fields at some certain angles $\phi_i = \phi_0 + \Delta\phi_i$ $(i = 1, 2, \cdots, P)$ are known. Here, ϕ_0 is a reference angle. Now we want to reconstruct the scattered information in the whole angle range approximately using the limited scattered data. In this work, we choose the Pade approximation because it can provide

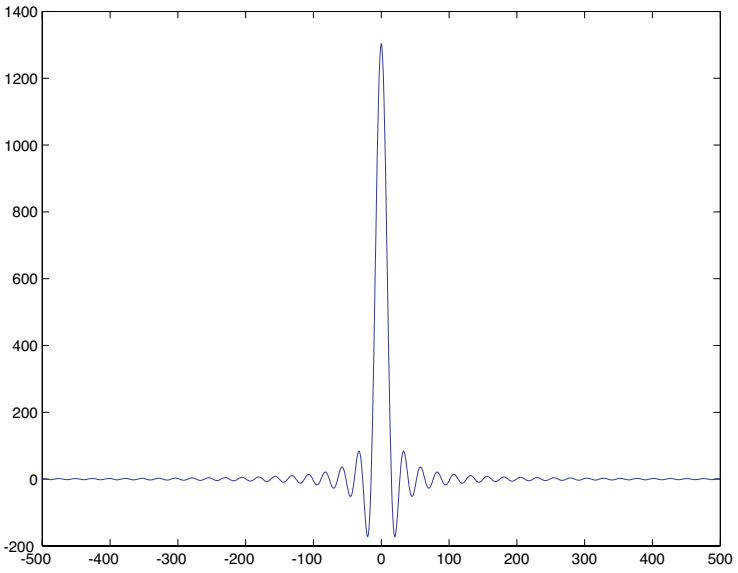

(a)

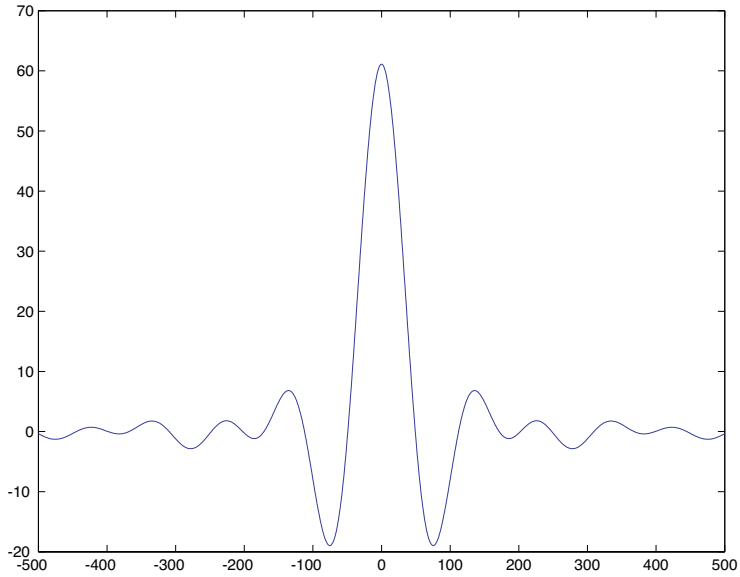

(b)

Figure 3. The curve of $\omega(\vec{R})$, where the horizontal axis represents R, and the vertical axis represents the function ω. (a) $a = 0$; (b) $b/a = 2.0$.

a good performance for oscillating functions, which has been widely used in the asymptotic waveform evaluation (AWE) technique for the frequency-domain electromagnetic analysis. In general, the scattered field in an arbitrary angle $\phi = \phi_0 + \Delta\phi$ can be expanded as

$$f(\phi_0 + \Delta\phi) = \frac{\sum_{m=0}^{M} a_m \Delta\phi^m}{1 + \sum_{n=1}^{N} b_n \Delta\phi^n}, \tag{8}$$

where the expansion coefficients $a_m (m = 0, 1, \cdots, M)$ and $b_n (n = 1, 2, \cdots, N)$ are unknown. Hence, there is a total of $M+N+1$ unknown parameters to be determined. In order to determine such unknowns, at least $P = M + N + 1$ scattered data are required:

$$f(\phi_0 + \Delta\phi_i) = \frac{\sum_{m=0}^{M} a_m \Delta\phi_i^m}{1 + \sum_{n=1}^{N} b_n \Delta\phi_i^n}, \tag{9}$$

in which $i = 1, 2, \cdots, P$. After simple derivations, the above equation is written as

$$\begin{bmatrix} 1, \Delta\phi_1, \ldots\ldots \Delta\phi_1^M, -\Delta\phi_1 f(\phi_1) \ldots\ldots, -\Delta\phi_1^N f(\phi_1) \\ 1, \Delta\phi_2, \ldots\ldots \Delta\phi_2^M, -\Delta\phi_2 f(\phi_2) \ldots\ldots, -\Delta\phi_2^N f(\phi_2) \\ \vdots \\ \\ \vdots \\ 1, \Delta\phi_P, \ldots\ldots \Delta\phi_P^M, -\Delta\phi_P f(\phi_P) \ldots\ldots, -\Delta\phi_P^N f(\phi_P) \end{bmatrix} \begin{bmatrix} a_0 \\ \vdots \\ a_m \\ b_1 \\ \vdots \\ b_n \end{bmatrix}$$

$$= [f(\phi_1), f(\phi_2), \ldots\ldots f(\phi_P)]^T, \tag{10}$$

where T denotes a conjugate. Clearly, the expansion coefficients can be obtained after solving the above matrix equation. Unfortunately, such a matrix equation is usually ill-conditioned, especially when the order of equations is larger than 40. In order to achieve a stable solution of the ill-posed problem, a Tikhonov regularization [18, 19] is used.

For easy implementation, the matrix equation (10) can be simply rewritten as

$$\overline{\mathbf{A}} \cdot \mathbf{x} = \mathbf{y}. \tag{11}$$

To seek the minimal norm solution to Eq. (11) by an optimization scheme, we consider the following object function

$$\mathcal{E} = ||\mathbf{y} - \overline{\mathbf{A}} \cdot \mathbf{x}||^2 + \delta ||\mathbf{x}||^2, \tag{12}$$

in which $||\cdot||$ is the norm of a vector. The regularization term in Eq.(12) is to ensure the norm of $\mathbf{x}$ not to be too large with the regularization parameter δ. Using the minimization technique, Eq. (12) is equivalent to the following matrix equation

$$(\overline{\mathbf{A}}^+ \cdot \overline{\mathbf{A}} + \delta \overline{\mathbf{I}}) \cdot \mathbf{x} = \overline{\mathbf{A}}^+ \cdot \mathbf{y}, \tag{13}$$

where $\overline{\mathbf{A}}^+$ is the conjugate transpose matrix of $\overline{\mathbf{A}}$, and $\overline{\mathbf{I}}$ is the unitary matrix. Because the matrix $\overline{\mathbf{I}}$ is well posed, the matrix $\overline{\mathbf{A}}^+ \cdot \overline{\mathbf{A}} + \delta \overline{\mathbf{I}}$ is also well posed. As a consequence, a stable solution of $\mathbf{x}$ will be obtained.

4. RECONSTRUCTION RESULTS

In order to test the validity of the proposed method, we first consider a circular PEC cylinder with radius $a = 1$ m. In such a simple case, the scattered magnetic fields can be computed exactly using the Mie series [17], which are regarded as the measured data. In this example, we mainly observe the influence of limited frequency band on the imaging. With the aid of the fast Fourier transform (FFT), the imaging results from Eq. (7) are illustrated in Figure 4. Here, full-angle information from 0 to π is used and different maximum frequencies are chosen to produce different resolutions.

From the FFT procedure [11], we have known that $\Delta x = \pi/k_{xm}$ and $\Delta y = \pi/k_{ym}$ if $-k_{xm} \le k_x \le k_{xm}$ and $-k_{ym} \le k_y \le k_{ym}$. Hence, the larger k_{xm} and k_{ym} are, the higher the imaging resolution is, as shown in Figures 4(a) and 4(b). On the other hand, the imaging region $D_x \times D_y$ is defined by $D_x = 2\pi/\Delta k_x$ and $D_y = 2\pi/\Delta k_y$. As a consequence, the less Δk_x and Δk_y are, the larger the imaging region is, as depicted in Figure 4(b).

For the cases of larger $k_{\min}$, for example, $k_{\max}/k_{\min} \approx 2.0$, the reconstruction results of the PEC circular cylinder are illustrated in Figure 5, where the full-angle information are again used. When $k_{\max} = 128.0$ and $k_{\min} = 70.0$, the imaging result is shown in Figure 5(a). When $k_{\max} = 256.0$ and $k_{\min} = 150.0$, the imaging result is shown in Figure 5(b). Comparing the two figures, we clearly see that the high-frequency information can produce a much better resolution if $k_{\max}/k_{\min}$ is fixed, which is coincident with the earlier analysis.

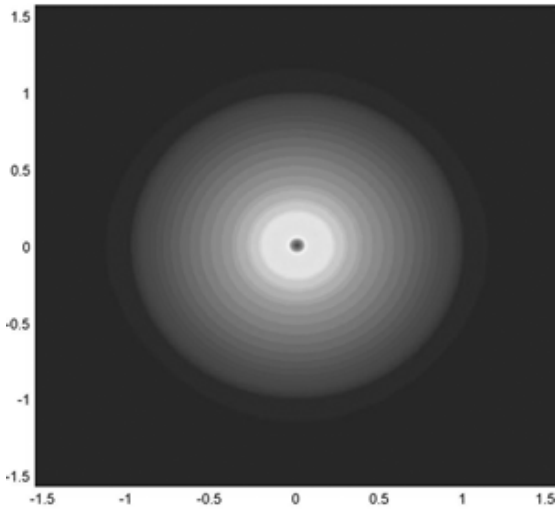

(a)

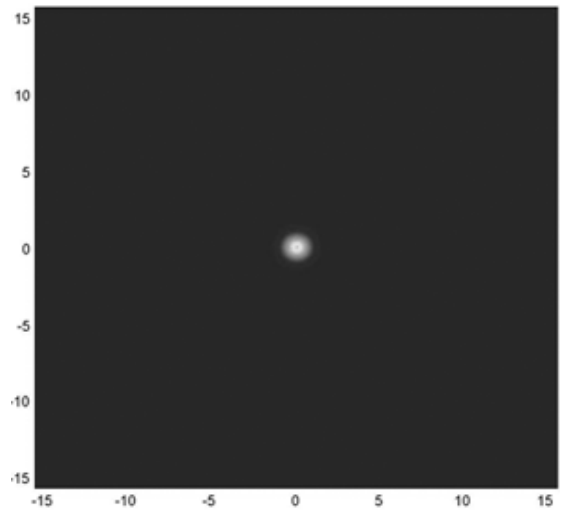

(b)

Figure 4. The reconstructed results of a PEC circular cylinder with radius $a = 1\,\text{m}$=1m, where the horizontal axis represents the x coordinate, and the vertical axis represents the y coordinate. (a) $k_{\max} = 32.0$, $k_{\min} = 1.0$, $\Delta k = 1.0$, and 32 frequencies have been used. (b) $k_{\max} = 25.6$, $k_{\min} = 0.1$, $\Delta k = 0.1$, and 256 frequencies have been used.

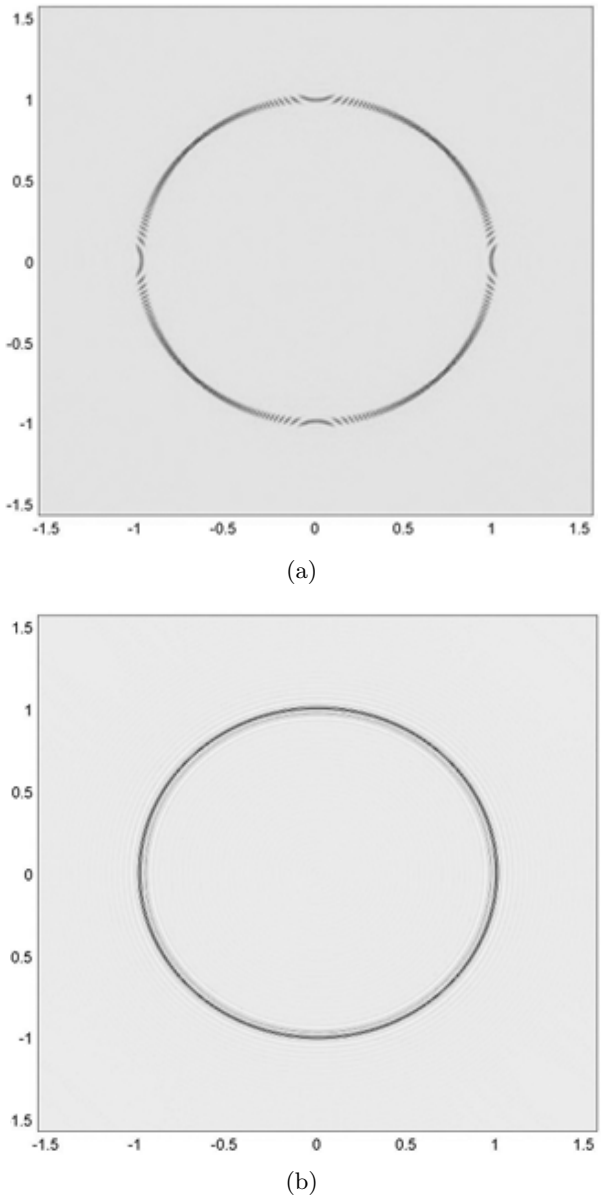

(a)

(b)

Figure 5. The reconstructed results of a PEC circular cylinder with radius $a = 1\,\mathrm{m}$=1m, where the horizontal axis represents the x coordinate, and the vertical axis represents the y coordinate. (a) $k_{\max} = 128.0$, $k_{\min} = 70.0$, and $\Delta k = 1.0$; (b) $k_{\max} = 256.0$, $k_{\min} = 150.0$, and $\Delta k = 1.0$.

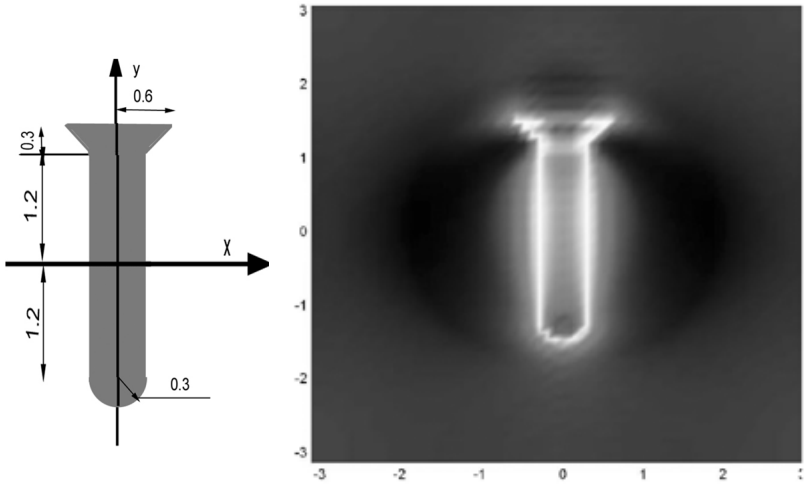

(a) (b)

Figure 6. The original model and the reconstructed image of a PEC missile. (a) The original model. (b) The imaging result with full incident angles.

Next, we consider the reconstruction of a PEC missile model shown in Figure 6(a). For such a model, the method of moments (MOM) has been applied to simulate the scattered data by adding 10 % white noise. When the whole scattered information for all incident angles around the target are involved, the imaging result is illustrated in Figure 6(b), where $k_{\max} = 16.0$, $k_{\min} = 0.5$, and 32 frequencies are used. Clearly, the missile target is well reconstructed with the full-angle information.

However, the full-angle information is hard to be obtained in practical applications. Suppose that we have four radars located at $\phi = 0$, $\pi/2$, π, and $3\pi/2$ to collect scattered data, and each radar can scan a maximum angle of $\pi/9$. Hence, only the scattered information in limited angles is available in this case: $\phi \in (-\pi/9, \pi/9) \cup (\pi/2 - \pi/9, \pi/2+\pi/9) \cup (\pi-\pi/9, \pi+\pi/9) \cup (3\pi/2-\pi/9, 3\pi/2+\pi/9)$. Clearly, we only know the scattered fields in a totally $8\pi/9$ angle range. The other scattered data in an angle range of $10\pi/9$ are unknown. If we simply ignore such scattered data, the imaging result is illustrated in Figure 7(a), where the head and bottom parts of the missile cannot be reconstructed. When we apply the Pade interpolation technique to recover the scattered data in the angle range of $10\pi/9$, the imaging result is shown in Figure 7(b). Clearly, the whole missile target is well

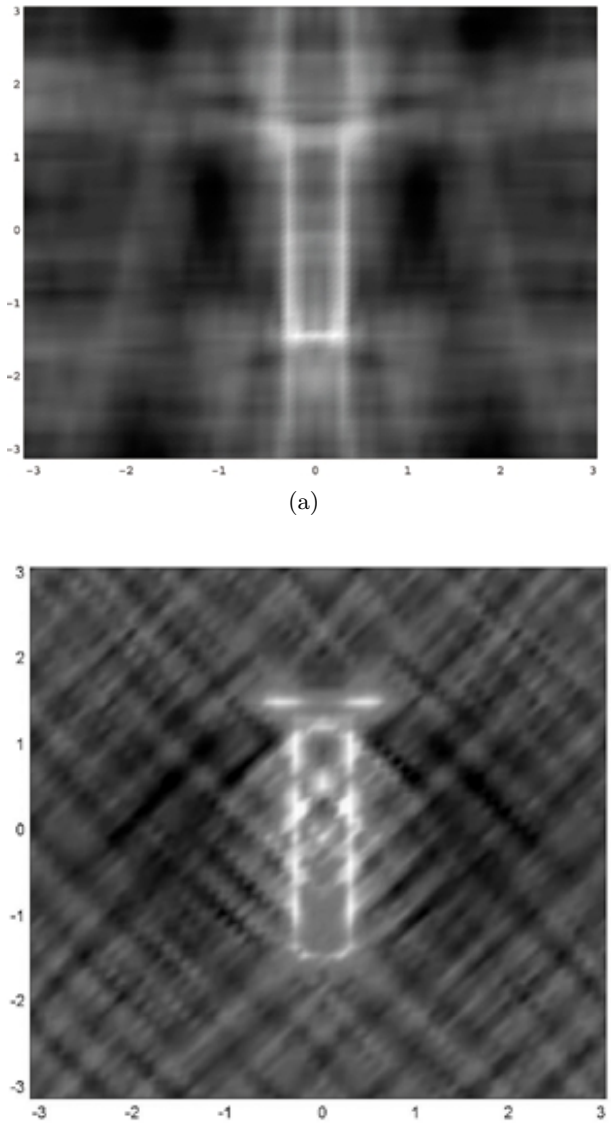

Figure 7. The reconstructed results of the PEC missile with limited incident anglesangle, where the horizontal axis represents the x coordinate, and the vertical axis represents the y coordinate. (a) Without using the Pade interpolation technique. (b) Using the Pade interpolation technique.

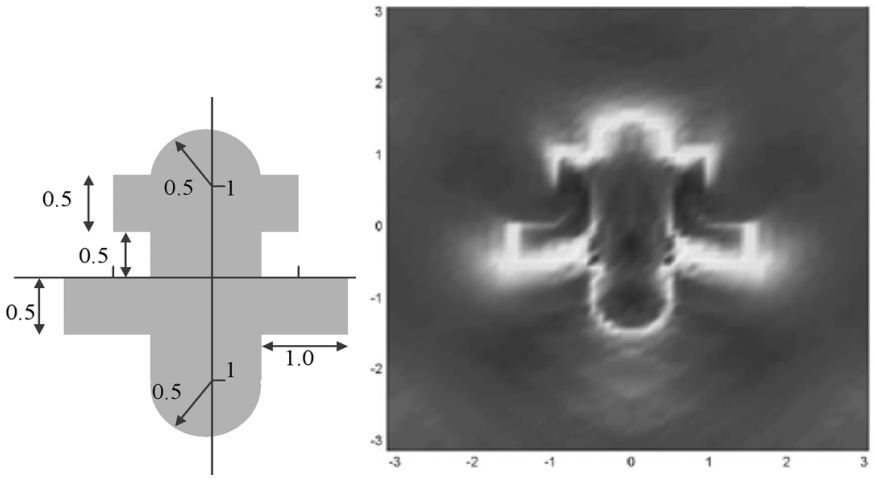

(a) (b)

Figure 8. The original model and the reconstructed image of a PEC aircraft. (a) The original model. (b) The imaging result with full incident angles.

reconstructed using the proposed method even though more than half angle information is unknown.

Finally we consider a complicated aircraft model as demonstrated in Figure 8(a). Again, MOM has been used to simulate the scattered data by adding 10% white noise. When the whole scattered field information for all incident angles around the target are known, the reconstruction result of the aircraft target is shown in Figure 8(b), where $k_{\max} = 16.0$, $k_{\min} = 0.5$, and 32 frequencies are used. Obviously, the aircraft is well reconstructed with the full-angle information. Similarly, if we only know the scattered fields in the limited angle range of $8\pi/9$ as listed in the above example, and ignore the other scattered information, the imaging result is shown in Figure 9(a). Clearly, the aircraft is hardly identified without using the Pade interpolation technique.

Figure 9(b) illustrates the radar image with limited angle incidences using the Pade interpolation technique, where the Tikhonov regularization is not applied ($\delta = 0$). From this figure, we can see that the reconstruction result is still poor due to the ill-posed problem. After adopting the Tikhonov regularization, however, the image quality has been greatly improved, as shown in Figure 10. Here, the regularization parameter is set as $\delta = 10^{-4}$. The above examples validate the efficiency of the proposed method.

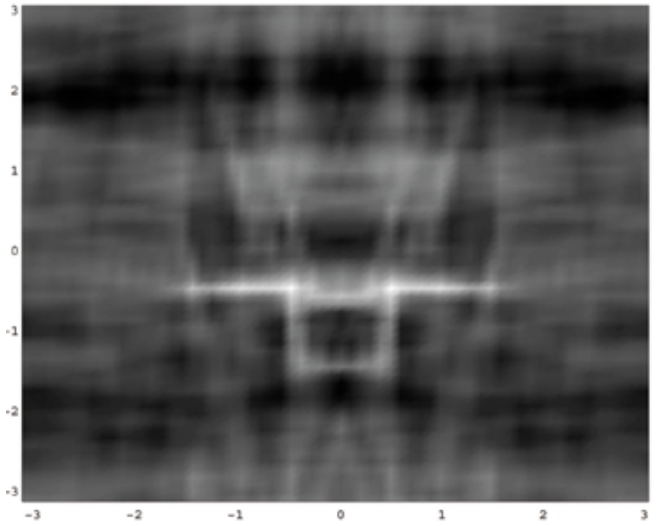

(a)

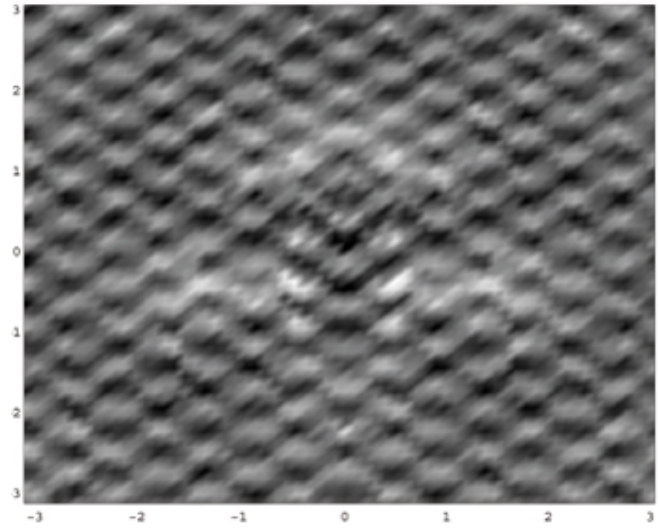

(b)

Figure 9. The reconstructed results of the PEC aircraft with limited incident angles. (a) Without using the Pade interpolation technique. (b) Using the Pade interpolation technique and $\delta = 0$.

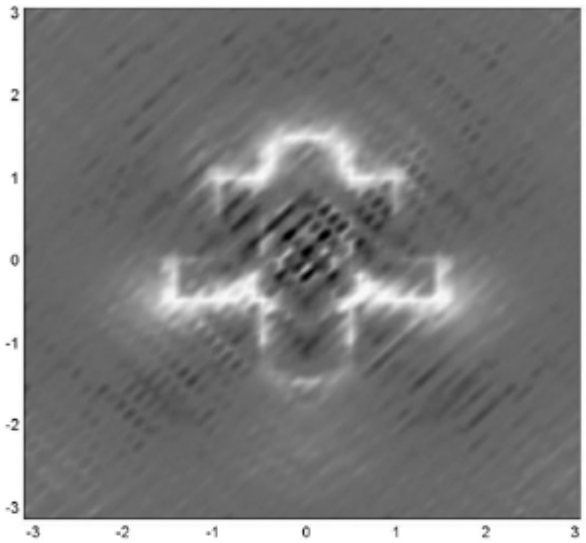

Figure 10. The reconstructed result of the PEC aircraft with limited incident angles using the Pade interpolation technique, where $\delta = 10^{-4}$.

5. CONCLUSIONS

In this work, we have proposed an efficient method to reconstruct the shape of 2D PEC targets using limited scattered information. From the theoretical analysis, all scattered-field data are required for the target imaging in the whole angle range (from 0 to 2π) and in the whole frequency range (from 0 to ∞). Obviously, such data are impossible in a practical application. To solve the problem, we have studied the influence of limited frequencies and limited incident angles on the quality of imaging, where the Pade interpolation technique with the Tikhonov regularization has been developed to obtain the scattered field information in the whole angle range from limited-angle information. Reconstruction examples have verified the validation and efficiency of the proposed method.

ACKNOWLEDGMENT

This work was supported by the National Science Foundation of China for Distinguished Young Scholars under Grant No. 60225001, and in part by the Selected Funding to Scientific Activity for Returnee.

REFERENCES

1. Lewis, R. M., "Physical optics inverse diffraction," *IEEE Trans. Ant. Propagat.*, Vol. 17, 308–314, Mar. 1969.
2. Das, Y., "On radar target shape estimation using algorithms for reconstruction from projections," *IEEE Trans. Ant. Propagat.*, Vol. 26, 274–279, Feb. 1978.
3. Bennett, C. L., "Time domain inverse scattering," *IEEE Trans. Ant. Propagat.*, Vol. 29, 213–219, Feb. 1981.
4. Bojarski, N. N., "A survey of the physical optics inverse scattering identity," *IEEE Trans. Ant. Propagat.*, Vol. 30, 980–989, 1982.
5. Boerner, W. M., C. M. Ho, and B. Y. Foo, "Use of Radon's projection theory in electromagnetic inverse scattering," *IEEE Trans. Ant. Propagat.*, Vol. 2, 336–341, March 1981.
6. Rothwell, E. J., K. M. Chen, D. P. Nyquist, and J. E. Ross, "Time-domain imaging of airborne targets using ultra-wideband or short-pulse radar," *IEEE Trans. Ant. Propagat.*, Vol. 43, 327–329, March 1995.
7. Dai, Y. C., E. J. Rothwell, K. M. Chen, and D. P. Nyquist, "Time-domain imaging of radar targets using algorithms for reconstruction from projections," *IEEE Trans. Ant. Propagat.*, Vol. 45, 1227–1235, August 1997.
8. Chan, C. K. and N. H. Farhat, "Frequency swept tomographic imaging of three-dimensional perfectly conducting objects," *IEEE Trans. Ant. Propagat.*, Vol. 29, 312–319, March 1981.
9. Young, J. D., "Radar imaging from ramp response signatures," *IEEE Trans. Ant. Propagat.*, Vol. 24, 276–282, May 1976.
10. Dural, G. and D. L. Moffatt, "SAR imaging to identify basic scattering mechanisms," *IEEE Trans. Ant. Propagat.*, Vol. 42, 99–110, January 1994.
11. Cui, T. J. and W. C. Chew, "Study of resolution and super resolution in electromagnetic imaging for half-space problems," *IEEE Trans. Ant. Propagat.*, Vol. 52, 1398–1411, June 2004.
12. Belkebir, K., A. Baussard, and D. Premel, "Edge-preserving regularization scheme applied to modified gradient method to reconstruct two-dimensional targets from data laboratory-controlled," *Progress In Electromagnetics Research*, PIER 54, 1–17, 2005.
13. Persson, K. and M. Gustafsson, "Reconstruction of equivalent currents using a near-field data transformation — with radome," *Applications Progress In Electromagnetics Research*, PIER 54,

179–198, 2005.

14. Bermani, E., A. Boni, A. Kerhet, and A. Massa, "Kernels evaluation of SVM-based estimators for inverse scattering problems," *Progress In Electromagnetics Research*, PIER 53, 167–188, 2005.
15. Chen, X., K. Huang, and X.-B. Xu, "Microwave imaging of buried inhomogeneous objects using parallel genetic algorithm combined with FDTD method," *Progress In Electromagnetics Research*, PIER 53, 283–298, 2005.
16. Thomas, V., J. Yohannan, A. Lonappan, G. Bindu, and K. T. Mathew, "Localization of the investigation domain in electromagnetic imaging of buried 2-D dielectric pipelines with circular cross section," *Progress In Electromagnetics Research*, PIER 61, 111–131, 2006.
17. Cockrel, C. R. and F. B. Beck, "Asymptotic waveform evaluation (AWE) technique for frequency domain electromagnetic analysis," NASA Technical Memorandum 110292, Nov. 1996.
18. Tikhonov, A. N. and V. Y. Arsenin, *Solution of Ill-Posed Problems*, V. H. Winston and Sons, Washington D.C., 1977.
19. Cui, T. J., Y. Qin, G. L. Wang, and W. C. Chew, "Low-frequency detection of 2D buried objects using high-order extended Born approximations," *Inverse Problems*, Vol. 20, S41–S62, 2004.